Book of Abstracts

Radisson Blu Royal Garden Hotel, Trondheim, April 9-11 2024

180°N

TABLE OF CONTENTS

Title **Page**

1

Reference tissue uptake of [18F]PSMA-1007 positron emission tomography

Bendik S Abrahamsen*[1], Ingerid S Knudtsen*[1], Andreas J Tulipan[2,3], Eivor Hernes[3], Trond Bogsrud[4,5], Kirsten M Selnæs[6], Håkon Johansen[6], Tone F Bathen†[1,6], Mattijs Elschot†[1,6]
*†*These authors contributed equally*

[1]Department of Circulation and Medical Imaging, Norwegian University of Science and Technology, Trondheim, Norway, [2]Nuclear Medicine/PET Centre, Department of Radiology, Haukeland University Hospital, Bergen, Norway, [3]Division of Radiology and Nuclear Medicine, Oslo University Hospital, Oslo, Norway, [4]PET Imaging Centre, University Hospital of North Norway, Tromsø, Norway, [5]PET-Centre, Aarhus University Hospital, Aarhus, Denmark, [6]Department of Radiology and Nuclear Medicine, St. Olavs Hospital, Trondheim, Norway

Introduction: Semi-quantitative uptake measurements are part of the PROMISE framework for interpretation of PSMA PET/CT of prostate cancer, where tumor uptake is compared to uptake in select reference tissues: blood pool, liver and parotid glands for the tracer [68Ga]Ga-PSMA-11. [18F]PSMA-1007 has primarily hepatobiliary excretion and it is suggested to use spleen as reference tissue instead of liver for this tracer. The aim of this study was to investigate the normal range of, and interpatient variability in, reference tissue uptake measurements for [18F]PSMA-1007 in prostate cancer patients, with particular focus on the splenic uptake.

Methods: A total of 102 PET/CT scans of prostate cancer patients with biochemical recurrence from three hospitals (St Olavs hospital, Haukeland University Hospital and University Hospital of Northern Norway) were included in the analysis. SUV_{mean} and SUV_{max} measurements were performed in the blood pool, spleen, and parotid glands according to a standardized protocol. Results are reported as median with 5^{th} and 95^{th} percentiles.

Results: Median SUV_{max} of the reference tissues were 1.2 [0.6, 2.2] for blood, 15.8 [8.9, 26.2] for spleen and, 26.6 [14.5, 40.4] for the parotid glands. Median SUV_{mean} were 11.9 [6.6, 20.7] for spleen and 19.3 [11.2, 32.1] for the parotid glands. SUV_{max} and SUV_{mean} were higher in the spleen than the parotid glands in 15/102 (14.7%) and 20/102 (19.6%) patients, respectively.

Conclusion: A substantial number of patients present with higher [18F]PSMA-1007 uptake in spleen than parotid glands. The clinical implications are unclear, but our result pinpoint that a number of patients will not fit into lesion categorization according to the PROMISE framework.

Note: The material presented in this abstract will also be submitted as part of an article to European Journal of Nuclear Medicine and Molecular Imaging (EJNMMI).

2

Interim 18F-FDG-PET-based combined dose and linear energy transfer escalation of proton therapy in head and neck cancer

Garrido-Hernandez, Guillermo[1], Ytre-Hauge, Kristian S[2], Winter, Rene M[1], Danielsen, Signe[3], Alsaker, Mirjam D[4], Boer, Redalen, Kathrine R[1], Henjum, Helge[2]

[1]Department of Physics, Norwegian University of Science and Technology, Trondheim, Norway, [2]Department of Physics and Technology, University of Bergen, Bergen, Norway, [3]Department of Oncology, St. Olav's Hospital, Trondheim University Hospital, Trondheim, Norway, [4]Department of Radiotherapy, Cancer Clinic, St. Olav's Hospital, Trondheim University Hospital, Trondheim, Norway

Purpose: To increase radiotherapy outcome of head and neck cancer, a combination of increased dose and increased linear energy transfer (LET) to aggressive tumor sub-volumes using proton therapy is attractive. With 18F-FDG-PET acquired at baseline and two weeks into treatment (interim) we defined the biological target volumes (BTV) for such a joint dose-LET escalation. We assessed the feasibility of interim adaptation of proton therapy plans by combined dose-LET escalation to the BTV and its effects to surrounding healthy tissue.

Materials/Methods: We used the semiautomated just-enough-interaction (JEI) segmentation method to delineate BTV from 18F-FDG-PET interim images acquired from nine HNC patients in treatment position. We assumed a correlation between tumor aggressiveness and high standardized uptake value (SUV) at interim to identify the BTV. We used the in-house Monte Carlo based recalculation and reoptimization system from University of Bergen to simulate optimized proton therapy plans with a constant relative biological effectiveness (RBE) of 1.1, delivering 68 Gy(RBE) in 34 fractions to the high-risk target volumes, a 10% dose escalation to the BTV and to deliberately increase the LET to the BTV.

Results: The JEI method identified the BTV at interim 18F-FDG-PET which allowed to adapt proton therapy. Dose-LET escalation proton plans resulted in LET increases to the BTV between 1.0 and 3.0 keV/µm for the near-maximum LET (LET2%) and between 0.7 and 2.0 keV/µm for the median LET (LETmedian). LET increases were also seen in the nearby organs and the clinical target volume (CTV) surrounding the BTV. Effects of LET increases in dose distributions resulted in an increase of the near-maximum dose (D2%) from 7.5 to 20.0 Gy(RBE), and of the median dose (Dmedian) from 9.0 to 14.0 Gy(RBE) in the BTV. Lower, but generalized increases in the dose metrics were also seen for surrounding organs (pharynx mucosa, larynx, oral cavity, parotid glands, spinal cord) and the clinical target volume (CTV) surrounding the BTV.

Conclusions: High quality interim 18F-FDG-PET enabled simulation of combined dose-LET optimized proton therapy plans and successfully increased both the dose and LET in the BTV after interim adaptation. We expect the precision in BTV segmentation and dose delivery to increase if hypoxia-PET images were available. Our current approach indicated that image-driven dose and LET escalation to tumor sub-volumes has the potential to improve the target dose distribution, and efficiently targeting potentially aggressive or radioresistant tumor tissue. However, the combined dose-LET escalation to the BTV resulted in potential dose increases to surrounding healthy tissues and should be considered carefully.

Keywords: Proton therapy, dose escalation, LET, FDG-PET

3

Intravoxel incoherent motion modelling of diffusion-weighted MRI using deep learning: simulations and evaluation in head and neck cancer

Amalie Toftum Hop[1], Marte Kåstad Høiskar[1], René M. Winter[1], and Kathrine Røe Redalen[1]

[1]*Department of Physics, Norwegian University of Science and Technology, Trondheim, Norway*

Purpose: Diffusion-weighted magnetic resonance imaging (DW-MRI) is a promising image modality for radiotherapy (RT) applications. Quantitative DW-MRI can be obtained by the intravoxel incoherent motion (IVIM) model, which separates tissue diffusion and perfusion-induced diffusion, and has the potential to predict and monitor treatment response. The model is described by three parameters: pure tissue diffusion coefficient Dt, perfusion fraction fp, and pseudo-diffusion coefficient Dp. However, these IVIM parameters are associated with poor precision and reproducibility. This becomes particularly relevant when only few diffusion-weighted images (b-value images) are included, a compromise often made in clinical protocols. Our aim was to compare three algorithms for IVIM modelling using just 5 b-value images as input: least squares fitting (LSQ), segmented fitting (SEG) and one self-supervised deep neural network (DNN), using simulations and clinical DW-MRI of head and neck cancer (HNC) patients.

Methods: Synthetic DWI-MRI signal series were simulated with 5 and 11 b-values by inserting pseudorandom IVIM parameter values into the IVIM model. The 11 b-values served as reference. Rician noise was added to the synthetic IVIM signals, generating data sets with different signal-to noise ratio (SNR) of 8 to 100. For each synthetic series of noisy IVIM signals, IVIM parameters were estimated with all three IVIM algorithms: LSQ, SEG and DNN. The accuracy of the estimated IVIM parameters was assessed by computing the normalised root-mean-square error (NRMSE). To evaluate the agreement between the estimated and synthetic IVIM signal curves, the root-mean-square error between the signal curves (signal-RMSE) was calculated. Finally, IVIM parameters were estimated in 68 tumours of 44 HNC patients. The IVIM parameter maps were compared visually and to signal-RMSE maps.

Results: In simulations with 11 b-values and SNR= 20 (Figure 1a), similar to the SNR in the patient data, the DNN showed higher accuracy (lower NRMSE) for all IVIM parameters, especially for Dp, compared to the LSQ and SEG algorithms, with NRMSE(Dt)= 0.18 vs 0.27/0.33; NRMSE(fp)= 0.22 vs 0.39/0.39; NRMSE(Dp)= 0.42 vs 0.78/0.89). When the number of b-values was reduced to 5 (Figure 1b), DNN maintained a higher accuracy than the fitting algorithms, especially for Dp, as shown by NRMSE(Dt)= 0.24 vs 0.32/0.29; NRMSE(fp)= 0.25 vs 0.47/0.35; NRMSE(Dp)= 0.56 vs 1.51/1.53). The median signal-RMSE was similar among all three algorithms, both when using 11 and 5 b-values. Figure 2 shows parameter maps of Dt, fp, and Dp calculated with LSQ, SEG, and DNN algorithms for a representative patient tumour. While all algorithms gave IVIM parameter maps with similar spatial pattern, DNN generated smoother maps with fewer unphysical values for fp and Dp than the LSQ and SEG algorithms. The median signal-RMSE over all tumors obtained with LSQ, SEG, and DNN algorithms were 0.01, 0.01, and 0.02, respectively.

Conclusion: DNN outperforms LSQ and SEG algorithms for IVIM modelling in simulations with both high and reduced number of b-values. It seems feasible to use DNN for IVIM modelling of DW-MRI with few b-values for HNC patients, which can help promote IVIM parameters as quantitative imaging biomarkers in future clinical protocols.

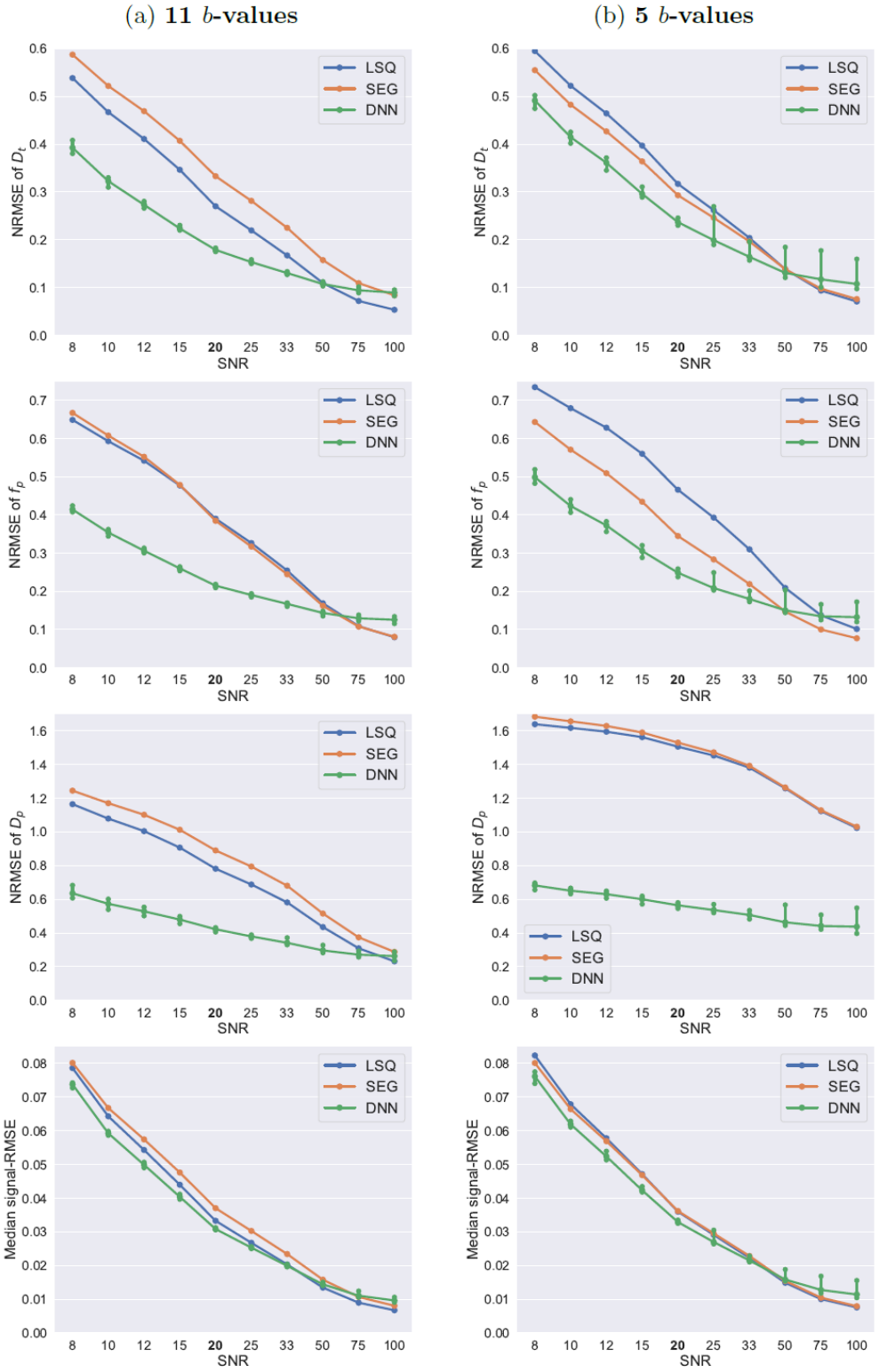

Figure 1: Results of the simulations. The NRMSE of the estimated D_t (first row), f_p (second row), and D_p (third row), and the signal-RMSE (fourth row), obtained with LSQ (blue), SEG (orange) and DNN (green) algorithms at different SNRs when using 11 (left column) and 5 (right column) *b*-values. The DNN was applied 25 times, and the point and error bars represent the median and the 2.5th to 97.5th percentile interval.

3

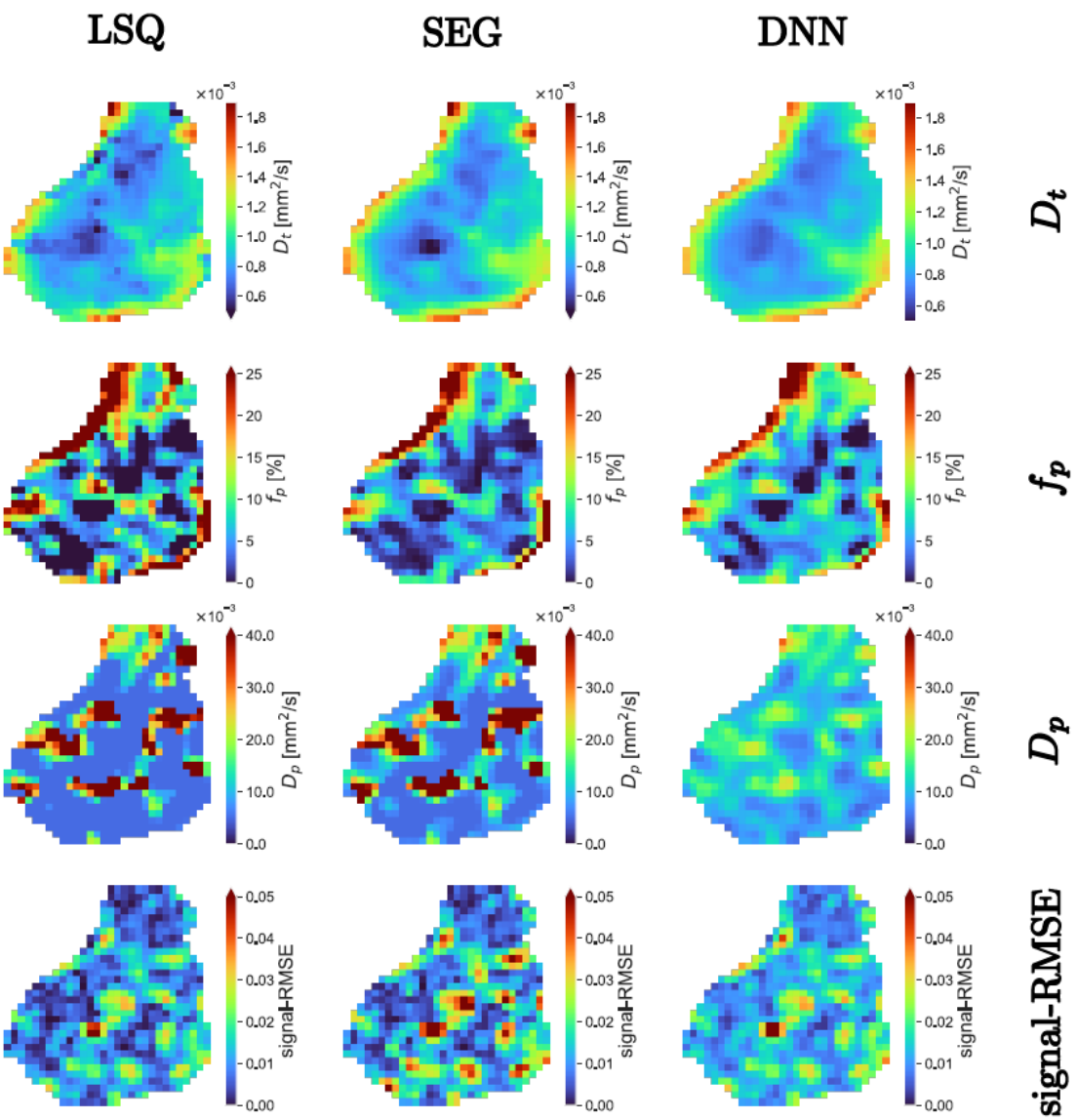

Figure 2: Parameter maps of D_t (first row), f_p (second row), and D_p (third row), and the signal-RMSE (fourth row) for a representative head and neck tumour slice. The parameters were estimated with LSQ (left), SEG (middle), and DNN (right column) algorithms.

4

Dosimetric evaluation of synthetic CT for PET/MR-only proton therapy of head and neck cancer

Marte Kåstad Høiskar[1], Natalie Hornik[1,2], Mirjam Delange Alsaker[3], Kajsa Fridstrøm[1,3], Sigrun Saur Almberg[3], Kathrine Røe Redalen[1], René M. Winter[1,*]
**Presenting author: René Winter, rene.winter@ntnu.no*

[1]Department of Physics, Norwegian University of Science and Technology, Trondheim, Norway, [2]Section for Biomedical Physics, Department of Radiation Oncology, University Hospital and Medical Faculty, Eberhard Karls University Tübingen, Tübingen, Germany, [3]Cancer Clinic, St. Olavs hospital, Trondheim University Hospital, Trondheim, Norway

Purpose: Planning computed tomography (pCT) is the primary image modality for photon and proton dose calculations in radiotherapy (RT) planning today. Magnetic resonance imaging (MRI) excels in soft tissue contrast, whereas positron emission tomography (PET) offers valuable functional or physiological information, making these attractive modalities for additional guidance of RT delineations or dose adaptations. It has been shown for photon therapy that an MR-derived synthetic CT (sCT) can replace the pCT for dose calculation, allowing for a workflow solely based on MRI. Such workflow can increase clinical efficiency, reduce patient time or CT patient dose, and enables hybrid PET/MR as a one-stop-shop for RT planning. However, also for proton therapy which is emerging, the dosimetric accuracy of sCT needs to be estimated before such workflow can be used in practice. Our aim was to investigate the feasiblity of MRI-derived sCT for proton planning in comparison to photon planning in a PET/MR imaging trial in head-and-neck cancer.

Methods: For 12 patients with HNC, PET/MRI and pCT were acquired in treatment position before treatment with photon therapy. Photon and proton plans were created in RayStation software based on the pCT, prescribing 68 Gy (34 fractions of 2 Gy) to the clinical target volume (CTV). Photon plans were the clinical plans made for all patients; proton plans were made retrospectively for six of the patients so far. For each patient, sCT was generated from T2-weighted MRI using a commercial neural network based software, MRIplanner (Spectronics, Sweden). The sCT was registered to the pCT using automatic rigid registration with manual correction in RayStation. Delineated volumes were copied from pCT to sCT, and pCT plans were recalculated on the sCT both for photons and protons, without re-optimisation. Dose volume histograms (DVHs) and global gamma index with passing criterion of 2%/2mm were analyzed to compare the spatio-dosimetric agreement between pCT and sCT dose distributions, both for photons and protons. A gamma index smaller than unity indicates that the dose agrees within the passing criterion.

Results: DVH metrics for pCT and sCT plans were similar for photon plans, but larger differences were seen for proton plans. Similarly, the gamma index analysis showed that the dose calculated with sCT compared to pCT differed more for protons than photons, resulting in larger regions with gamma index above 1 (Figure 1). The mean gamma passing rate (Figure 2), defined as the percentage of points satisfying the condition gamma index < 1, was 92 ± 5 % for photons and 77 ± 9 % for protons, indicating a larger spatio-dosimetric discrepancy between sCT and pCT plans for protons.
We are currently analyzing if patient positioning, registration inaccuracies or sCT inaccuracies in the mouth region can explain some of the discrepancies between sCT and pCT dose distributions, especially for protons.

Conclusion: Preliminary results indicate that MRI-derived sCT is feasible for a PET/MRI-only workflow for HNC photon therapy, but not for protons. Whether the dose discrepancy seen with protons originates from the sCT or methodological limitations needs further investigation.

4

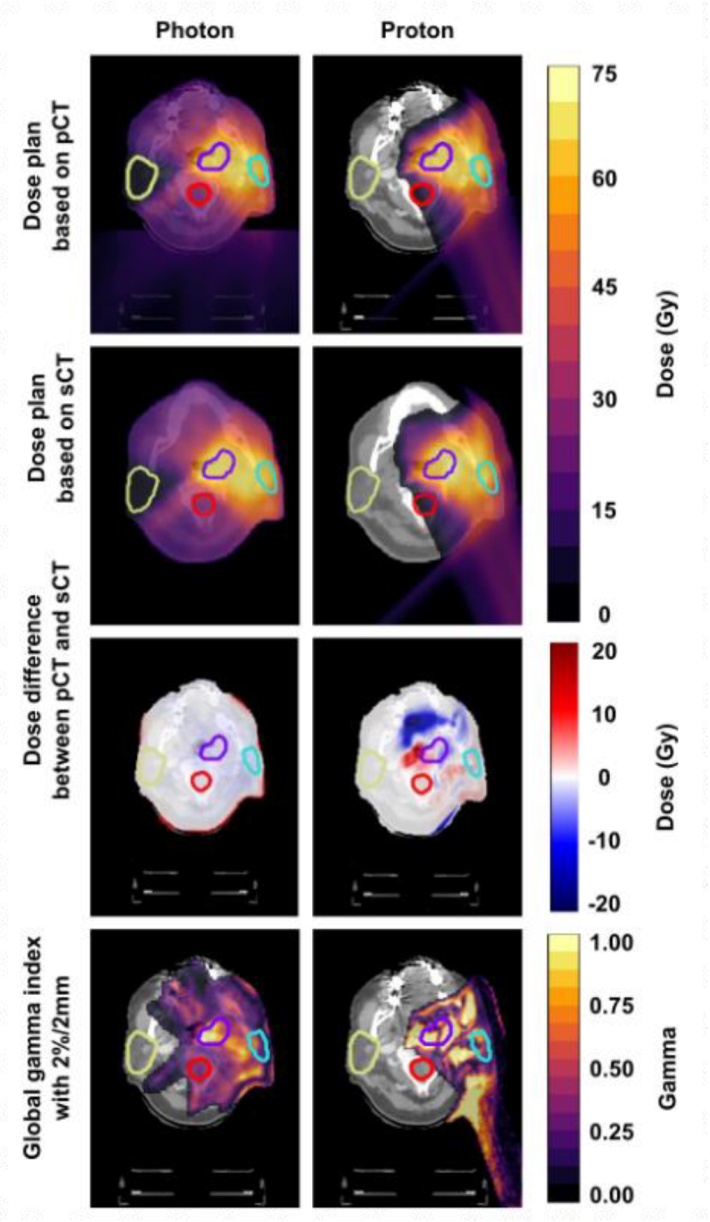

Figure 1: Photon (left) and proton plans (right) were created using planning CT (pCT, top row) and recalculated for synthetic CT (sCT, second row). Based on the dose difference (third row) between the pCT and sCT plans, a distribution of gamma index with criterion of 2 %/2mm (bottom row) was calculated. One image slice of one representative patient was used. The purple, red, yellow and blue delineations are the CTV, spinal cord, parotid sin and parotid dx, respectively.

4

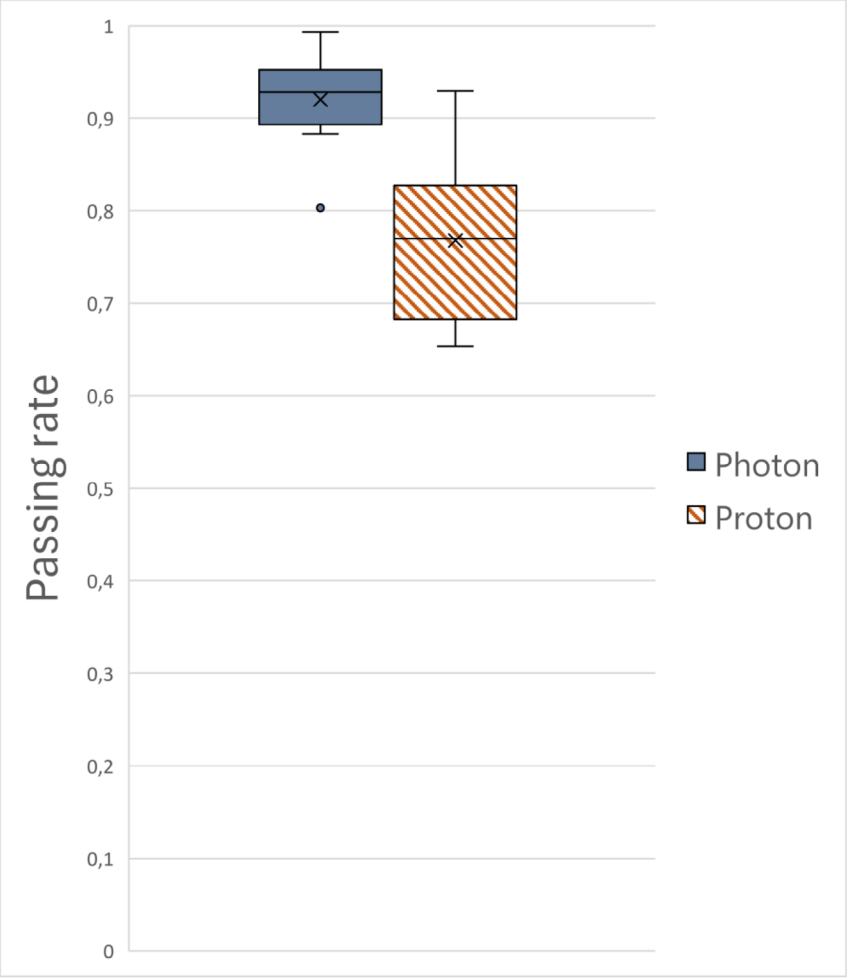

Figure 2: Boxplot of the patients' passing rates with 2 %/2mm gamma criterion for photons (blue) and proton (red, striped) plans.

5

Evaluation of FAPI 74 radiotracers' stability and biodistribution in preclinical murine models

Sindhu Kancherla, Mathias Kranz, Kristin Lode, Yngve Guttormsen, Rodrigo Berzaghi, Angel Moldes-Anaya and Inigo Martinez-Zubiavrre

Background: FAPI PET radiotracers are a family of FAP-targeting molecules labeled with positron-emitting radionuclides, such as ^{18}F or ^{68}Ga. Upon administration, these radiotracers preferentially bind to FAP-expressing fibroblasts within the tumor microenvironment. Their selective uptake allows high-contrast images showing the distribution of FAP-positive cells, which correlates with the presence and extent of a variety of cancers. Despite its extensive use in both clinical and preclinical settings, the *in vivo* stability and biodistribution properties have not been properly documented in preclinical models. In this work we evaluate [^{18}F]FAPI-74 and [^{68}Ga]FAPI-74 radiotracers stability and biodistribution in different mouse strains.

Methodology: NOTA-FAPI-74 precursor and standard was generously supplied by SOFIE Ltd. We have established protocols for radiolabeling of the NOTA-FAPI-74 precursor with both ^{18}F or ^{68}Ga. Radiotracer stability has been tested in murine plasma samples *ex vivo* and upon administration into healthy C57Bl6 and Balb-c animals. Blood samples were collected at different time-points and the amount of intact tracer were measured by HPLC-RAD-PDA. Additionally, dynamic PET scans were conducted to characterize the radiotracer kinetics, clearance, and organ biodistribution.

Results: Both [^{18}F]FAPI-74 and [^{68}Ga]FAPI-74 show good radiotracer stability in *ex vivo* tests performed on murine plasma samples at 37 °C for as long as 120 min. *In vivo* metabolism studies show a rapid defluorination of the [^{18}F]FAPI-74 tracer occurring already 1 min and 5 min post injection, with values ranging between 50 % and 30 % of intact tracer (upon > 90 % extraction efficiency). Interestingly, the levels of intact radiotracer remain rather stable in the circulation at longer time points, up to 60 min.Dynamic PET/MRI with [^{18}F]FAPI-74 in the two mouse strains presents a rapid clearance of the radiotracer from circulation through renal elimination as shown by high accumulation in kidneys and urinary bladder. Uptake in the bone structures can be assigned to early defluorination as demonstrated by the *ex vivo* plasma analysis.

Conclusions: This study shows for the first time an unexpected rapid defluorination of [^{18}F]FAPI-74 after iv. injection in murine models. These observations are utterly relevant for preclinical research done with [^{18}F]FAPI-74, indicating that most of the signal observed from static scanstudies may correspond to free fluorine. We are currently investigating the *in vivo* stability of FAPI-74 radiolabeled with ^{68}Ga.

References:

Dahl K, Jussing E, Bylund L, Moein MM, Samén E, Tran T. Fully automated production of the fibroblast activation protein radiotracer [18 F]FAPI 74. J Label Compd Radiopharm. 2021 ; 64: 346 352.

6

68Ga/177Lu-PSMA theranostics in recurrent high-grade glioma: First study results & future perspectives

A. Karlberg[1,2], B. E. Vindstad[2], , E. M. Berntsen[1,2], H. Johansen[1], T. M. Keil[1], O. Solheim[5,6], S. Kjærnes Øen[1], T. Skeidsvoll Solheim[3,4] and L. Eikenes[2]

[1]Department of Radiology and Nuclear Medicine, St. Olavs Hospital, Trondheim University Hospital, [2]Department of Circulation and Medical Imaging, Norwegian University of Science and Technology, [3]Cancer clinic, St. Olavs Hospital, Trondheim University Hospital, [4]Department of clinical and molecular medicine, Faculty of Medicine and Health Sciences, Norwegian University of Science and Technology, [5]Department of Neurosurgery, St. Olavs hospital, Trondheim University Hospital, [6]Department of Neuroscience, Norwegian University of Science and Technology, Trondheim, Norway.

Background and aim: Patients with recurrent high-grade glioma have a very poor prognosis and no effective standard therapy. In the current study, 68Ga/177Lu-PSMA theranostics is evaluated as a treatment alternative to improve existing diagnostic and therapeutic methods in glioma management, and possibly increase the overall survival and quality of life for this patient group. The overall aim is to evaluate the safety, tolerability and efficacy of 177Lu-PSMA therapy in recurrent high-grade gliomas. A secondary aim is to compare the pre-therapeutic tumor uptake of 68Ga-PSMA to the tumor absorbed doses from 177Lu-PSMA to establish an appropriate indication for therapy. This is one of the first studies in the world exploring theranostics as a treatment alternative for patients with brain tumors.

Materials and methods: Eligible patients with a positive 68Ga-PSMA-PET/MRI examination are selected for 177Lu-PSMA treatment (maximum 6 cycles, 6-8 weeks intervals). The patients are carefully monitored during each treatment cycle (PET/MR, SPECT/CT, neurological tests, blood tests, and quality of life questionnaires). Two patients with CNS WHO grade 4 glioblastomas have been included in this ongoing study. Both patients received standard treatment with surgery, radiotherapy and chemotherapy prior to inclusion, and were left with no other treatment options at recurrence. 177Lu-PSMA (7.1-7.3 GBq) was administered intravenously (Patient A: 1 treatment, Patient B: 3 treatments) and SPECT/CT scans were performed for dosimetry.

Results: 68Ga-PSMA-PET prior to treatment demonstrated tumor uptake in both patients (SUV_{max_A}:9.0 and SUV_{max_B}:4.4) as well as uptake in the parotid glands (SUV_{max_A}:21.8 and SUV_{max_B}:15.9). 68Ga-PSMA uptake in normal brain was low, yielding high TBR (TBR_A: 136.0 and TBR_B: 45.4). Post treatment SPECT/CT revealed a rapid wash-out of activity, resulting in low absorbed doses (A: Tumor 1.4 Gy, kidneys 2.0-2.1 Gy, parotid glands 1.1-1.4 Gy, B: Tumor 2.6-2.9 Gy, kidneys 2.4-3.7 Gy, parotid glands 1.7-3.6 Gy). The patients reported no subjective side effects of the treatment, apart from transient xerostomia. Based on radiological evaluation (MRI), both patients demonstrated stable disease during the treatment cycles (third cycle not yet evaluated).

Conclusion: Despite low tumor doses, the radiological stability of disease in these two patients is promising. An innovative approach to boost brain tumor doses is to use intraarterial (IA) administration instead of intravenous (IV) administration. This could potentially provide a better treatment effect in these patients, compared to IV administration. We will apply for a change in the study protocol to use IA administration in selected patients in the current study, in collaboration with Erasmus University Medical Center (Erasmus MC) in Rotterdam.

7

From Liquid Target Production to Synthesis of [^{45}Ti]Ti-DOTA

Chubina P. Kumarananthan[1], Unni A. Kvitastein[1], Tamal Roy[2], Camillo Bruhn[2], Erwan Le Roux[2], Tom C. H. Adamsen[1,2]

[1]Department of Radiology, Haukeland University Hospital, Bergen, Norway, [2]Department of Chemistry, University of Bergen, Bergen, Norway

Introduction: ^{45}Ti (β+: 85 %) has medium long half-life ($t_{1/2}$ = 3.08 h) and low maximum positron endpoint energy (Emax = 1040.1 keV).[1] This makes it an excellent candidate for PET-imaging due to its potential to image slower physiological processes with high spatial resolution. The path from the radiochemistry to the clinical use of ^{45}Ti has been lengthy, likely due to its hydrolytic instability and high oxophilicity.[2] Stabilization of the radiometal through chelation is therefore crucial. This study uses a macrocyclic chelator, 1,4,7,10- tetraazacyclododecane-1,4,7,10-tetraacetic acid (DOTA), which is widely used in radiochemistry and deemed incompatible for titanium.[3] The aims are to (1) produce high activities of ^{45}Ti using a liquid target, (2) extract ^{45}Ti by solid phase extraction (SPE) or liquid-liquid extraction (LLE), and (3) complex ^{45}Ti with DOTA.

Materials and Methods: Liquid target irradiation were conducted by bombarding Sc(NO3)3 (0.5 – 2.5 M) in HNO3 (0.05 – 0.3 M) with 14.3 MeV protons to follow the natSc(p,n)^{45}Ti reaction. The irradiations were performed in a PETtrace 860 cyclotron with varying irradiation times (1 – 4 h) and beam currents (15 – 35 µA). A hydroxamate resin (ZR^{TM}) was utilized in an automated SPE, with oxalic acid (1 M), citric acid (1 M) and citrate (1 M) as eluents. Some oxalic acid eluates were further purified on a quaternary ammonium anion-exchange resin (QMA).[4] For the LLE-method, a mixture of guaiacol and anisole (9/1) (v/v) served as the organic phase in a manual extraction process.[5] The phases were mixed by shaking and separated using a centrifuge. Complexation was carried out by mixing either the eluates or organic phases with a DOTA-solution (in DMSO w/pyridine) for 20 min at 90 °C.

Results: ^{45}Ti was produced in various amounts with activities ranging from 0.2 to 4 GBq at end of bombardment (EOB) (n = 70, RNP: 94.7 – 99.8 %). Gamma-ray spectrometry analysis indicated that radionuclidic impurities, mostly 44Sc, were rinsed out during the extractions. In the LLEs, ^{45}Ti was extracted into the organic phase with an extraction efficiency (EE) of 31.8 – 81.1 % (n = 3). Some LLEs resulted in an incomplete phase separation, likely due to the concentration of Sc(NO3) and HNO3, as well as the irradiation parameters. However, radioHPLC analysis of the crude reaction mixture from the satisfactory LLEs indicated the successful formation of [^{45}Ti]Ti-DOTA (radiochemical conversion (RCC): 96.8 – 99.5 %). The ZR-resin effectively retained ^{45}Ti, and the EE ranged from 5.9 to 64.3 % (n =16) where oxalic acid was most efficient. A basic wash before elution increased the EE, nonetheless, the trans-chelation with DOTA was not evident for any of the eluents.

Conclusion: The liquid target productions of ^{45}Ti yielded activities up to 4 GBq; sufficient for studying separation and complexation with DOTA. While both the LLEs and SPEs extracted ^{45}Ti, the LLE-method notably facilitated the formation of the [^{45}Ti]Ti-DOTA complex. These results are significant for developing and using of [^{45}Ti]Ti-DOTA based tracers in PET imaging. Further work involves automating and optimizing the LLE process and purifying the complex for use in preclinical studies.

7

References:

1. Kuhn, S.; Spahn, I.; Scholten, B.; Coenen, H. H. Positron and γ-ray intensities in the decay of 45Ti. Radiochimica Acta 2015, 103 (6), 403-409. DOI: 10.1515/ract-2014- 0006.*****
2. Giesen, K.; Spahn, I.; Neumaier, B. Thermochromatographic separation of 45Ti and subsequent radiosynthesis of [45Ti]salan. Journal of Radioanalytical and Nuclear Chemistry 2020, 326 (2), 1281-1287. DOI: 10.1007/s10967-020-07376-2.
3. Pedersen, K. S.; Baun, C.; Nielsen, K. M.; Thisgaard, H.; Jensen, A. I.; Zhuravlev, F. Design, Synthesis, Computational, and Preclinical Evaluation of ^{nat}Ti/^{45}Ti-Labeled Urea-Based Glutamate PSMA Ligand. Molecules 2020, 25(5), 1104. DOI: 10.3390/molecules25051104
4. Holland, J. P.; Sheh, Y.; Lewis J. S. Standardized methods for the production of high specific-activity zirconium-89. Nuclear medicine and biology 2009, 36(7), 729–739, DOI: 10.1016/j.nucmedbio.2009.05.007
5. Pedersen, K. S.; Imbrogno, J.; Fonslet, J.; Lusardi, M.; Jensen, K. F.; Zhuravlev, F. Liquid–liquid extraction in flow of the radioisotope titanium-45 for positron emission tomography applications. Reaction Chemistry & Engineering 2018, 3 (6), 898-904. DOI: 10.1039/c8re00175h.

8

[13N]Ammonia - Rapid fire production of [13N]AMMO

Ole H Kvernenes[1], Tom CH Adamsen[1,2]

[1]Centre for Nuclear Medicine, Department of Radiology, Haukeland University Hospital, Bergen, Norway, [2]Department of Chemistry, University of Bergen, Bergen, Norway.

Aim: To set up and validate a fast and simple, cassette based, production of [13N]ammonia, yielding multiple doses of finished product, compliant with PhEur specifiactions.

Methods: The production of [13N]ammonia is performed by bombarding a 5 mM EtOH in H_2O (PhEur, WFI) in a dedicated target. The irradiated solution is transfered to a Neptis synthesis module vi a a target switch system. The synthesis, or more accurately the purification of {13N]ammo was done by using a modified [18F]NaF method and cassette, from Ora (Neuville, Belgium) and ABX (Radeberg, Germany) respectively, using the Ora Neptis Mosaic-RS synthesis module. The target solution was pushed through a QMA, in order to trap eventual anionic impurities before the [13N]ammonia is captured on a waters CM cartridge. After washing with sterile water, the CM cartridge is flushed with saline and the purified [13N]ammonia is collected in a product vial, via a sterile filter. The QMA and CM cartridges are flushed with sterile water, and the process can be repeated for a new batch of target solution.

Results: An experiment was set up, to examine how many batches we could produce using the same synthesis cassette. A full QC analysis, including HPLC identification, half life, HPGe spectroscopy, pH and endotoxin was performed on each batch. Sterility was performed on a pool of all batches. For each cassette we ran 9 sub-batches, including QC, and the experiment was repeated three times. It was evident from the data that a total of 5 sub-batches could successfully be produced from each cassette., with good results. A clear trend emerged that from sub batch 6 and onward, the ammonia was no longer captured on the CM cartridge and the final product activity was very low. We found this drop in activity to correlate with a clear drop in the pH, and pH did in fact fail for the latter batches.

Conclusion: A fast and simple, cassette based, production of [13N]ammonia has been achieved yielding a finished product, compliant with specifications stated in the European Pharmaocopeia. Each cassette can be used for a total of 5 batches of [13N]ammonia.

9

Robust, versatile, and interpretable deep learning model for prediction of the arterial input-function in dynamic [^{18}F]FDG-PET imaging of mice

Luigi Tommaso Luppino[1], Fredrik Aspheim[1], Kristoffer Wickstrøm[1], Michael Christian Kampffmeyer[1], Rodrigo Berzaghi[2,3], Rune Sundset[2,3], Robert Jenssen[1], and Samuel Kuttner[1,2,3]

[1]UiT Machine Learning Group, Department of Physics and Technology, UiT The Arctic University of Norway, Tromsø, Norway, [2]The PET Imaging Center, University Hospital of North Norway, Tromsø, Norway, [3]Nuclear Medicine and Radiation Biology Research Group, Department of Clinical Medicine, UiT The Arctic University of Norway.

Introduction: Dynamic positron emission tomography (PET) is a non-invasive imaging technique that quantifies biological processes in vivo. These can be quantitatively measured through tracer kinetic modelling, given that an arterial input-function (AIF), the radioactivity in arterial blood over time, is available. Arterial cannulation in small animals is, however, a complex and terminal surgery which is laborious, time-consuming, and hampered by limited blood volume. Proxies such as population-based AIF, imagederived input-function, or simultaneous estimation might require a blood sample for calibration, lack the necessary precision, or have other limitations. To overcome these issues, our group previously developed a novel, non-invasive deep learning-derived input-function (DLIF) model to estimate the AIF from dynamic PET data. Nonetheless, this model has its own shortcomings: sensitivity to input noise, no real blood sampling available for ground truth, strict input size requirements, fixed timing with respect to the injection, and no concrete insights nor understanding of the model's inner behaviour. Hereby, we aim not only to improve the DLIF model performance but also to address these shortcomings.

Methods: A prospective dataset of 53 mice was used for training. As input, dynamic [^{18}F] Fluorodeoxyglucose ([^{18}F]FDG) PET scans were reconstructed as 41 3D-volumes spanning over 45 minutes (25x5s, 9x20s, 7x300s). Random Gaussian noise was added to these volumes to increase the model's robustness. As ground truth, simultaneous and continuous arterial blood sampling yielded the AIF curves. A 3D-ResNet was used to extract spatial features by compressing each time step's 3D volume into one vector. These vectors were then stacked over time and fed into several 1D convolutional layers to extract temporal features and predict the AIF. The fully convolutional design of our model allows flexibility in input volume sizes, time series length, and input-function starting point. To increase trust and insight into the model's inner-workings, post-training analysis using the gradient-based approach GradCAM was conducted, yielding the saliency maps that highlight the important part of the input for the model's output. Starting from a given point of the output curve, it is possible to trace the gradients throughout the network all the way back to the input volumes, where the gradients will condense the most in those voxels deemed salient by the network.

Results: The results indicate that the model performs well, with the predicted input-functions closely following the ground truth. Further analysis indicate that the model is agnostic to time shifts and relaxes previous methods' requirements regarding input data size. The saliency maps suggested that the model correctly focuses on the vena cava in early time frames and the heart and kidneys in the latest stages, in line with our intuition of the animals' physiology and the tracer kinetics.

Conclusion: In this work we have developed a reliable, robust and interpretable deep learning model that predicts the input-function from dynamic PET images, without the need for manual interaction. With further validation, this could potentially overcome the need for arterial blood sampling in future small-animal [^{18}F]FDG PET imaging studies.

10

In situ radiolabeling technique for liposomal nanocarriers

Elena Markova[1], Morten Karlsen[2], Rune Sundset[1,3], Nataša Škalko-Basnet[4], Sjoerd Hak[5]

[1]Department of Clinical Medicine, Faculty of Health Sciences, UiT The Arctic University of Norway, Tromsø, Norway, [2]PET center, St. Olavs Hospital, Trondheim, Norway, [3]PET Imaging Center, University hospital of North Norway, Tromsø, Norway, [4]Department of Pharmacy, Faculty of Health Sciences, UiT The Arctic University of Norway, Tromsø, Norway, [5]SINTEF Industry, Department of Biotechnology and Nanomedicine, and Department of Circulation and Medical Imaging, Faculty of Medicine and Health Sciences, Norwegian University of Science and Technology, Trondheim, Norway.

Liposomes are attractive vehicles for delivering therapeutic agents due to their versatility, biocompatibility, and ability to encapsulate a wide range of compounds. Long circulating liposomal nanocarriers have been shown to accumulate in solid tumors, transporting chemo- and radio-therapeutics directly to cancerous tissue, thereby enhancing efficacy and decreasing dose-limiting side-effects.[1] Labeling liposomes with radionuclides allows for better understanding of their biodistribution, pharmacokinetics, in vivo stability, and targeting efficiency. ^{64}Cu is one of the few useful metallic positron-emitting radionuclides with a relatively long half-life (12.7 h), permitting studies to be performed for as long as 48 h after administration, which is ideal for following the biodistribution of long circulating liposomes.[2] Well-established coordination chemistry of copper allows for utilization of a variety of chelator systems that can be linked to suitable molecules, such as lipids, which would allow for chelator incorporation into the liposomal membrane.[3] Here, we present a fast and efficient chelator-based liposome radiolabeling strategy, entailing incorporation of NODAGA-conjugated lipid (DSPE-NODAGA) into the liposome membrane and subsequent radiolabeling with ^{64}Cu.

Liposomes for radiolabeling were prepared using the thin-film hydration (TFH) method, with the following lipid composition DSPC:Cholesterol:DSPE-PEG2k:DSPE-NODAGA 61:33:5:1 mol%, respectively. Liposomes were hydrated using 10 mM HEPES, 150 mM NaCl, pH 7.4, to form a suspension with 30 mM final lipid concentration and then extruded. Liposomes were characterized for size, polydispersity index (PDI), and ζ potential using dynamic light scattering. Liposomes (100 µl) were radiolabeled using 30 µl ^{64}CuCl2 solution in 0.1 M ammonium acetate, pH 5.67, at 24 °C (~71 mBq radioactivity). Radiochemical yield (RCY) was determined by both NAP-5 columns, radio-TLC, and HPLC with SEC. Stability of radiolabeling in buffer was examined using radio-TLC, whereas radiolabeled liposomes stability in mouse serum was explored using HPLC with SEC.

Liposomes size was 110 ± 2 nm, PDI ≤ 0.05, and ζ potential 11 ± 3 mV with no significant change after radiolabeling. Liposome radiolabeling was almost instant, with 100 % RCY after 5 min co-incubation of 30 mM liposomes with ^{64}Cu solution at 24 °C. The minimal total lipid concentration to obtain 100 % RCY was 3.8 mM. RCY remained stable at 100 % even after 20 h at room temperature. In the lower concentration range (1.88 and 0.94 mM), RCY increased by 1.3x after 20 h. RCY remained unchanged upon exposure to mouse serum, after 1 and 20 h co-incubation of radiolabeled liposomes with mouse serum.

In summary, the presented fast and efficient liposome radiolabeling strategy holds great promise for advancing our understanding and utilization of liposomal nanocarriers in biomedical research and clinical practice. Our approach of using NODAGA-coupled lipid can be translated to other types of lipid nanoparticles. The nearly instantaneous radiolabeling process, coupled with high radiolabeling efficiency and stability, demonstrates the robustness and reliability of this approach. Furthermore, the observed stability of radiolabeled liposomes in mouse serum highlights the potential for in vivo applications.

10

Acknowledgements: This study was financed by the 180°N (Norwegian Nuclear Medicine Consortium) project and Tromsø Forskningsstiftelse (19_PET-NUKL)

References:

1. Hansen, A.E., Petersen, A.L., Henriksen, J.R., Boerresen, B., Rasmussen, P., Elema, D.R., Rosenschöld, P.M.A., Kristensen, A.T., Kjær, A. and Andresen, T.L., 2015. Positron emission tomography based elucidation of the enhanced permeability and retention effect in dogs with cancer using copper-64 liposomes. ACS Nano, 9(7), pp.6985-6995.
2. Lewis, J.S., Laforest, R., Dehdashti, F., Grigsby, P.W., Welch, M.J. and Siegel, B.A., 2008. An imaging comparison of 64Cu-ATSM and 60Cu-ATSM in cancer of the uterine cervix. Journal of Nuclear Medicine, 49(7), pp.1177-1182.'
3. Shokeen, M. and Anderson, C.J., 2009. Molecular imaging of cancer with copper-64 radiopharmaceuticals and positron emission tomography (PET). Accounts of chemical research, 42(7), pp.832-841.

11

Exploring the Potential of ^{45}Ti in PET Imaging: Formation and Assessment of the Ti-DOTA Complex

Eduard Pogorilyy[1], Tamal Roy[1], Erwan Le Roux[1]

[1]*Department of Chemistry, University of Bergen, Bergen, Norway*

Among the relatively efficient radiometals, the radionuclide titanium-45 isotope, stands out as a radionuclide of interest for its beneficial qualities in Positron Emission Tomography (PET). This isotope is notable for its high positron emission rate (85 %) coupled with a relatively low average kinetic energy of positrons, leading to both reduced radiation doses for patients and enhanced image resolution. Additionally, its half-life of ca. 3.1 hours is advantageous in clinical settings, allowing for imaging procedures to be conducted several hours post-injection, thereby simplifying logistical considerations, for instance. The production of ^{45}Ti in substantial quantities is feasible through the 45Sc(p,n)45Ti reaction.

The expansion of the collection of chelators capable of efficiently binding non-radioactive Ti4 ions indeed represent a significant scientific objective.1 In this work, we present the proof-of-concept that the ligand DOTA (1,4,7,10-tetraazacyclododecane 1,4,7,10-tetraacetic acid) can form a complex with the Ti^{4+} ion (Figure 1). Formation of the Ti-DOTA complex was confirmed through a range of advanced analytical methods that together validated both the successful formation and detailed analysis of the Ti-DOTA complex.

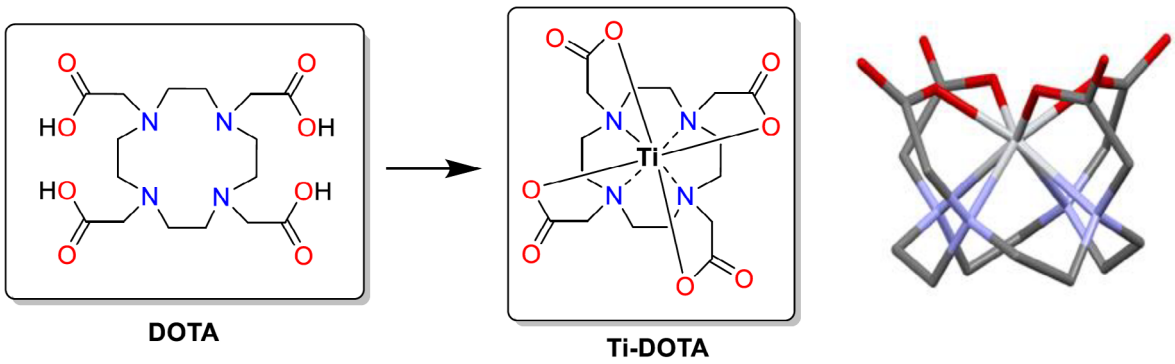

Figure 1: Synthesis of nonradioactive titanium complex of DOTA.

Following the production and detailed examination of the complex, we conducted a series of in vitro metal competition studies, as the result, it was observed a low level of demetallation of Ti-DOTA complex. This evaluation demonstrated that Ti-DOTA complex is highly suitable for use in PET-imaging.

References:

1. Boros E., Packard A. B. Radioactive Transition Metals for Imaging and Therapy. Chem. Rev. 2019; 119: 870–901.
2. Costa P., Metello L. F., Alves F., Naia M. D. Cyclotron Production of Unconventional Radionuclides for PET Imaging: the Example of Titanium-45 and Its Applications. Instruments 2018; 2:8.
3. Pogorilyy, E. Radiometal Based on Titanium-45 for PET-Imaging. Master thesis, University of Bergen, 2021, P. 1-95.

12

Application of a visual classification method for novel tau tracer [^{18}F]MK-6240 in MCI and AD patients

Peter Wessel Strandhagen[1], Vere Rose Megens[1], Live Eikenes[2], Asta Håberg[1]

[1]Department of Neuromedicine and Movement Science, Norwegian University of Science and Technology, [2]Department of Circulation and Medical Imaging, Norwegian University of Science and Technology

Background: Alzheimer's disease (AD) is a progressive, neurodegenerative disorder that is considered the most prevalent form of dementia. Tau protein is central in the development of AD, wherein neurofibrillary tangles (NFTs) along with amyloid plaques constitute the hallmark pathologies of the disease. The second-generation positron emission tomography (PET) tracer [^{18}F]-MK6240 (Lantheus) detects and quantifies NFTs in AD patients with high specificity. Despite the presence of NFT aggregation associated with Braak stages and deterioration of cognitive impairment, patients' spatial distribution of NFTs varies. Shuping et al., 2023 have developed a visual classification method (VCM) from 1 to 4 for uptake of the [^{18}F]-MK6240 tracer, where '1' classifies patients with no tracer uptake, '2' represents uptake in medial temporal lobe (MTL) only, '3' represents uptake in MTL and neocortex and '4' represents uptake outside MTL. The objectives of this study were firstly to confirm the feasibility of the VCM described by Shuping et al., 2023, and secondly to compare the patient group in the current study regarding distribution between the 4 visual classifications with differences in age and clinical diagnosis.

Methods: [^{18}F]-MK6240 PET tracer images from 43 participants (mean age 70) diagnosed with MCI, mild dementia (MD) due to AD, AD, other/unknown cause of dementia (OU) or with no diagnosis yet (NO) were first visually assessed and categorised according to the four-class VCM from Shuping et al., 2023. The classified PET images among the 4 categories were then compared by their average age and clinical diagnosis.

Results: Of the 43 included patients, 7 (16 %) were categorised as 'no uptake', 13 (30 %) as 'MTL only', 21 (49 %) as 'MTL and neocortical', and 2 (5 %) as 'outside MTL'. Regarding age distribution, the 'no uptake' group had the lowest mean age (M = 68) of all the groups, whereas the 'MTL only' group had the highest (M = 72, F (3,39) = 1.02, p = 0.38). Regarding clinical diagnosis, 18/21 in the 'MTL and neocortical' group had a clinical diagnosis (7 MD, 7 MCI, 4 AD, 1NO, 2OU). The ´MTL and neocortical´ group also included the most AD patients compared to the other groups. In the 'no uptake' group, 3/7 did not have a diagnosis (3 NO, 3MCI, 1 AD). The 'MTL only' group did not include any AD patients (4 MD, 5 MCI, 1 NO, 3 OU).

Discussion: In our dataset, all cases could be successfully classified into the categories of the VCM. Most patients were assigned to the two categories including MTL uptake (79 %). This corresponds with diagnostic staging literature regarding AD on NFT deposition in the MTL. Interestingly, the 'MTL only' category did not include any AD patients, but rather patients diagnosed with MD or MCI. Accordingly, AD prodromal stages may be confined to NFT aggregation in the MTL but expand to cortical regions during disease progression. The 'no uptake' group consisted of 3 patients without a diagnosis (3/7), which might imply that these patients are at a prodromal stage where NFT aggregation has not commenced.

13

^{67}Cu produced at a biomedical cyclotron for preclinical in vivo studies

Ursula Søndergaard[1,2,3*], Thomas K Ekaney[1], Mathias Kranz[1,2], Rune Sundset[1,2], Kristina S Pedersen[3], Angel Moldes-Anaya[1,2], Mikael Jensen[3]

[1]The PET Imaging Center, University Hospital of North Norway, Tromsø, Norway, [2]Department of Clinical Medicine, UiT The Arctic University of Norway, Tromsø, Norway, [3]Hevesy Laboratory, DTU Health Technology, Technical University of Denmark, Risø, Denmark.

Background: The demand for ^{67}Cu is high due to recent developments in radioendotherapy and theranostics. With 100 % β^--emission, a half-life of 61.83 h and a dose point kernel similar to that of the clinically established ^{177}Lu [1], ^{67}Cu is ideal for radionuclide therapy. In addition, with positron-emitter ^{64}Cu having a half-life allowing tumour-dosimetry and excellent imaging properties, precision medicine theranostics is enabled, a constellation rarely present. In this study, we aimed to establish ^{67}Cu production at a biomedical cyclotron via the ^{70}Zn(p,α)^{67}Cu nuclear reaction, suitable for *in vivo* animal experimentation.

Method & Materials: Bombardments were performed at 16.5 MeV nominal incoming proton energy (GE PETTrace 860). Target electrodeposition was based on a method by Engle et al. [2]. Scaling up from test runs, enriched ^{70}Zn (97.5 %) was electrodeposited to a target thickness of 50 mg/cm^2, and bombarded for either 4 or 12 hours at respectively 60 and 40 µA. On the next day, the target was dissolved in 6 M HCl, evaporated to dryness and reconstituted in metal-free water. Solid phase extraction (SPE) was applied for final purification using two commercially available resins in series, TK200 and CU-resin (Triskem). Activity measurements and assessment of radionuclidic purity were done via γ-ray spectrometry. Non-radioactive metal content in the final product was assessed by ICP-OES. Radiolabelling was performed by adding PSMA-617 (70µL, 20nmol) in metal-free H_2O to 300µL $^{67}Cu^{2+}$ reconstituted in NaOAc buffer (pH 4.6) in a glass vial, mixing thoroughly and incubating at 90°C for 10 min. The final product was formulated in isotonic saline after purification by C18 SPE (Waters), i.v. injected (5.1 MBq) into a healthy C57BL6 mouse (12 weeks, 21.5 g) and subsequently SPECT imaged (40s/ projection,50 ROR, Trifoil SPECT CT) 1h, 24h, 48 and 72h.

Results: Maximum produced EOB activity reached to date was 120 MBq, of which 94 % was recovered for radiolabelling and *in vivo* testing. Radionuclidic purity at start of synthesis was > 99.4 %. Specific activity of purified ^{67}Cu end product varied from 144-573 MBq/ug in scale-up experiments. The radiochemical yield of ^{67}Cu-PSMA-617 was 94 % after final evaporation and reconstitution in saline. Biodistribution (Figure 1) with SPECT revealed high uptake in kidneys and liver followed by a washout phase.

Conclusion: We have established production of ^{67}Cu. The product quality is suitable for preclinical investigations, showing that the capabilities of biomedical cyclotrons can be explored for producing radiometals of therapeutic interest.

13

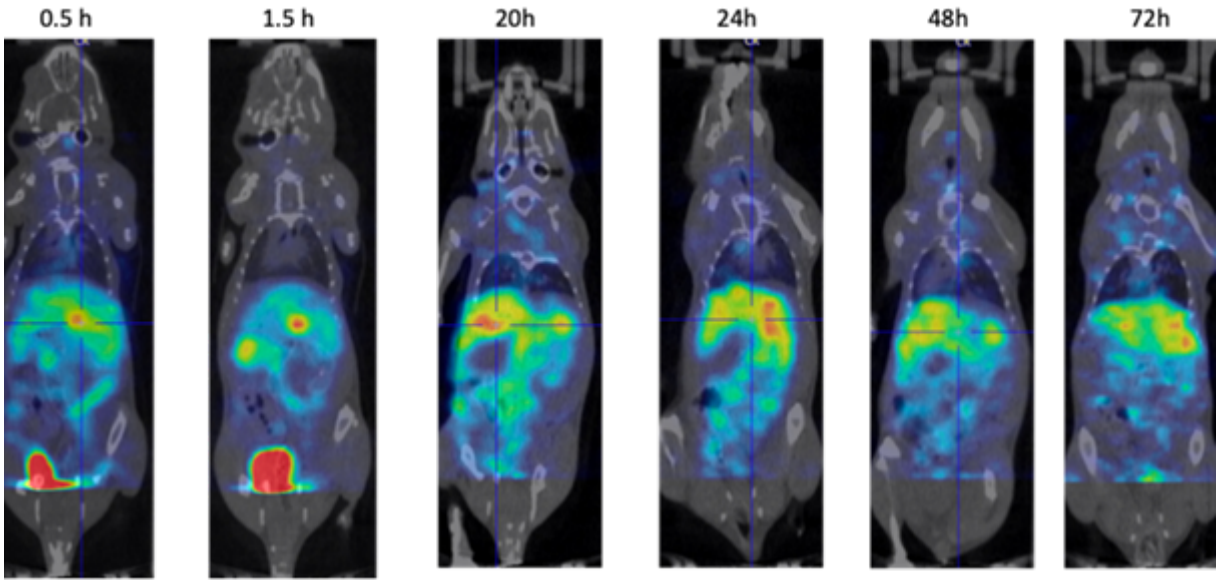

Figure 1. Kinetic micro-SPECT/CT/MR of a healthy mouse injected with 67Cu-PSMA-617

Acknowledgements: Dr. Samuel Kuttner is gratefully acknowledged for assisting with the SPECT calibrations to 67Cu. This work has in parts received funding from the European Union's Horizon 2020 research and innovation programme under grant agreement No 101008571 (PRISMAP - https://www.prismap.eu/about/project/) and in part from HelseNord (https://www.helse-nord.no/forskning-og-innovasjon/)

References:

1. Graves SA, Lopez-Rodriguez V, Gaspar-Carcamo RE, Valdovinos HF, Valle-Gonzalez M, Trejo-Ballado F, Severin GW, Barnhart TE, Nickles RJ, Avila-Rodriguez et al. Dose point kernels for 2,174 radionuclides. Med Phys 2019; 46:5284-5293.
2. Engle JW, Lopez-Rodriguez V, Gaspar-Carcamo RE, Valdovinos HF, Valle-Gonzalez M, Trejo-Ballado F, Severin GW, Barnhart TE, Nickles RJ, Avila-Rodriguez MA. Very high specific activity ^{66}/^{68}Ga from zinc targets for PET. Appl Radiat Isot. 2012; 70:1792-1796

14

Histomolecular validation of [18F]FACBC uptake in gliomas using image-localized biopsies

Benedikte Vindstad[1], Anne Jarstein Skjulsvik[2,3], Lars Kjelsberg Pedersen[4], Erik Magnus Berntsen[1,5], Ole Solheim[6,7], Tor Ingebrigtsen[4,8], Ingerid Reinertsen[1,9], Håkon Johansen[5], Live Eikenes[1], Anna Karlberg[1,5].

[1]Department of Circulation and Medical Imaging, Norwegian University of Science and Technology, Trondheim, [2]Department of Pathology, St. Olavs Hospital, Trondheim University Hospital, Trondheim, [3]Department of Clinical and Molecular Medicine, Faculty of Medical and Health Sciences, Norwegian University of Science and Technology, Trondheim, [4]Department of Neurosurgery, University Hospital of North Norway, Tromsø, [5]Department of Radiology and Nuclear Medicine, St. Olavs Hospital, Trondheim University Hospital, Trondheim, [6]Department of Neurosurgery, St. Olavs hospital, Trondheim University Hospital, Trondheim, [7]Department of Neuroscience, Norwegian University of Science and Technology, Trondheim, [8]Department of Clinical Medicine, Faculty of Health Sciences, UiT the Arctic University of Norway, Tromsø, Norway, [9]Department of Health Research, SINTEF Digital, Trondheim, Norway.

Purpose: Gliomas have a heterogeneous nature, and identifying the most aggressive parts of the tumor as well as defining tumor borders are important for histomolecular diagnosis, surgical resection and radiation therapy planning. This study evaluated [^{18}F]FACBC PET for glioma tissue classification, and the radiotracer's ability to delineate tumor volumes in comparison to ce-T1 MRI.

Methods: Patients with suspected primary or recurrent glioma were prospectively included from November 2019 to June 2021. Pre-surgical [^{18}F]FACBC PET/MRI was acquired, and the images were used during surgery and image-localized biopsy sampling of image-localized biopsies from each patient. Using ROC analysis, [^{18}F]FACBC tumor-to-background ratios (TBR) were compared to histomolecular results in each biopsy to determine optimal threshold values, sensitivity, specificity, and AUC values for correct classification of tumor tissue. PET volumes were determined in patients with glioblastoma based on the optimal threshold, to compare with ce-T1 volumes.

Results: A total of 48 biopsies from 17 patients were analyzed. ROC analysis found that despite low uptake in non-glioblastoma tumors, [^{18}F]FACBC TBR had higher sensitivity for classification of tumor tissue and high-grade tumor tissue than ce-T1 MRI. Additionally, [^{18}F]FACBC TBR was an excellent classifier for IDH1 wildtype tumor tissue with an AUC of 0.83 (95 % CI: 0.71 – 0.96). In glioblastoma patients, tumor volumes determined from [^{18}F]FACBC PET were on average 8 times larger than ce-T1 volumes and had a sensitivity of 87.5 % for tumor-positive biopsies compared to 31.5 % for ce-T1 MRI, with one false positive compared to two for ce-T1 MRI.

Conclusion: [^{18}F]FACBC PET demonstrated higher sensitivity for detection of tumor tissue than ce-T1 MRI, particularly in glioblastomas. The addition of [^{18}F]FACBC PET to conventional MRI could improve tumor classification and volume delineation. This has potential to further improve surgical resection and radiation therapy in primary and recurrent gliomas.

15

Targeting Arginase-1 with Liposomal nor-NOHA: A Novel Approach to Cancer Immunotherapy

Camilla Wolowczyk[1], Elena Markova[2], Alexandros Marios Sofias[3], Sjoerd Hak[4,5], Nataša Škalko-Basnet[6]

[1]Department of Biomedical Laboratory Science, Faculty of Natural Sciences, NTNU, Trondheim, Norway, [2]Department of Clinical Medicine, Faculty of Health Sciences, UiT The Arctic University of Tromsø, Norway, [3]Institute for Experimental Molecular Imaging, RWTH Aachen University, Germany, [4]Department of Biotechnology and Nanomedicine, SINTEF Industry, Trondheim, Norway, [5]Department of Circulation and Medical Imaging, Faculty of Medicine and Health Sciences, NTNU, Trondheim, Norway, [6]Department of Pharmacy, UiT The Arctic University of Tromsø, Norway

Introduction: Despite the great effort and promising pre-clinical results, only a small number of liposomal formulations have reached the clinic and had an impact on cancer patients. Several limitations of using liposomal formulations in this context are known, including the rapid recognition and clearance by phagocytic immune cells.[1] During tumor progression, cancer cells secrete several factors that result in infiltration of various immune cells, amongst other phagocytes. Here, we attempt to exploit these two traits by developing liposomal drug formulations with increased specificity towards tumor-infiltrating phagocytic immune cells to improve anti-cancer immune responses. Phagocytic immune cells such as neutrophils and myeloid-derived suppressor cells (MDSC) are responsible for arginase-1 (Arg1) overexpression in cancer.[2] Through arginine depletion this can result in suppression of T cell cytotoxicity and T cell anergy. High Arg1 expression is also associated with poor patient outcome, making Arg1 an interesting candidate to target. In this work we develop liposomes loaded with Arg1 inhibitor Nω-Hydroxy-nor-L-arginine (nor-NOHA) to potentially improve the drug efficacy.

Methods: nor-NOHA-loaded liposomes were prepared by thin-film hydration (TFH) using the following lipid composition; DSPC:Cholesterol:DSPE-PEG2k 62:33:5 mol %, respectively. After characterizing the liposomes, encapsulation efficiency (EE %), release profiles and cell cytotoxicity was assessed. Arginase inhibition was examined on differentiated bone marrow-derived macrophages (BMDM), using LC-MS/MS to measure arginine/ornithine ratios.

Results: The liposomes had a z-average <140 nm, PDI ≤ 0.12, and ζ potential ≥ -13 mV. EE % ranged from 6-9 %. In vitro release studies revealed a sustained release profile. Cytotoxicity assays demonstrated minimal toxicity. Also, nor-NOHA in liposomes inhibited Arg1 activity to the same extent as nor-NOHA in solution in BMDM, as evident from the significantly increased arginine/ornithine ratios in both cell lysates and medium.

Conclusion: In conclusion, our results show that liposomal formulations can encapsulate nor-NOHA. Sustained release profile, minimal cytotoxicity and robust Arg-1 inhibition suggest the potential of liposomal nor-NOHA as a safe and effective treatment option.

References:

1. Shi, J., Kantoff, P., Wooster, R. and Farokhzad, O. Nature Reviews Cancer. 2017. 17; 20
2. Grzywa, T.M., Sosnowska, A., Matryba, P., Rydzynska, Z., Jasinski, M., Nowis, D. and Golab, J. Frontiers in immunology. 2020. 11; 938